ACSNANO

www.acsnano.org

ARTICLE

Flexible Aggregation-Induced Emission-Active Hydrogel for On-Site Monitoring of Pesticide Degradation

Xu Yan,*[,∇] Tuhui Wang,[∇] Hongxia Li, Lening Zhang, Hua Xin, and Geyu Lu*

Cite This: https://doi.org/10.1021/acsnano.2c06544

Read Online

ACCESS | Metrics & More | Article Recommendations | Supporting Information

ABSTRACT: Benefiting from the stimuli-responsive property and powerful loading capacity, functionalized hydrogels are favorable for the fabrication of sensing devices. Herein, we design aggregation-induced emission (AIE)-active hydrogel discs by embedding gold nanoclusters@zeolite-like imidazole framework (AuNCs@ZIF) composites in double-network hydrogels to build a sensitive pesticide biosensor. The hydrogel discs integrate an AIE effect of AuNCs, a stimuli-responsive property of ZIF, and a porous network structure of the hydrogel, which enhances the sensing sensitivity via boosting the stable fluorescent signal and antifouling performance. In conjunction with a homemade device, the fluorescence images of hydrogel discs could be transduced into data information for accurate quantification of chlorpyrifos pesticide with a detection limit of 0.2 ng/mL. The dynamic degradation of chlorpyrifos in Chinese cabbage is demonstrated to confirm the practical application of hydrogel discs. Such AIE-active hydrogel discs could be a plant health sensor for the on-site quantification of pesticide residues on crops, holding great promise for precision agriculture.

KEYWORDS: *Hydrogel discs, Aggregation-induced emission, Zeolite-like imidazole framework, Biosensor, Pesticide degradation*

INTRODUCTION

Functionalized hydrogels with porous polymeric networks, biomimetic activity, and excellent tailorability have aroused increasing attention in a multifarious fascinating field, ranging from biomedical engineering[1−5] to electronics devices[6−9] and tailored biosensing.[10−14] The introduction of different types of fluorescent indicators (e.g., quantum dots,[15] carbon dots,[16] and dye[17]) inspired by nature (sea pansies and jellyfish) endows the hydrogels with stimuli-responsive properties. Fluorescent hydrogels integrate light-emitting properties and gel characteristics to facilitate the fabrication of actuators and point-of-care (POC) devices for expanding their bioapplication.[18−20] At present, one main barrier to the application of fluorescent hydrogels is the well-known aggregation-caused quenching (ACQ) effect.[21] Hydrogels with semisolid or condensed-state characteristics can inevitably restrict in motion spacing of fluorescent indicators during the gelation process, resulting in the limit of photoluminescence. To circumvent this problem, the concept of aggregation-induced emission (AIE) has been demonstrated successfully, bringing a tremendous impact on the traditional view.[22−24] More specifically, chromophores that hold the AIE effect emit weak fluorescence or are nonemissive in the monodispersed state, while they are intensively photoluminescent in the aggregated or intramolecular restricted state. In particular, gold nanoclusters (AuNCs) have been observed to perform the AIE effect via restraining intramolecular movement, greatly enriching the AIE element type.[25−27] Such a feature of AIE luminescence makes hydrogels have many distinct functions including gelation-induced emission and multimodality luminescence, rendering it possible to fabricate advanced smart materials. Actually, unlike solids and suspensions, a hydrogel holds a special aggregate state that causes AIE photoluminescent components (organic compounds or AuNCs) to exhibit unusual luminescence behaviors.[21,28,29] The hydrogel may possess a weak restrictive effect of chromophores for the formation of AIE due to its huge porous networks. Furthermore, the stability of chromophores is susceptible to the solution environment

Received: July 3, 2022
Accepted: October 19, 2022

(organic solvents, pH, etc.). Given the above limitations, the pursuit of fabricating an AIE-active hydrogel with excellent photoluminescence and good stability has great significance in designing stimuli-responsive sensors.

Generally, embedding AuNCs into nano- or microporous nanomaterials is proposed to achieve AIE luminescence by spatial confinement effects. Zeolite-like imidazole framework (ZIF) nanomaterials constructed by assembling metal ions with organic ligands, featuring a desirable pore structure with a rational design, are promising candidates for AuNC immobilization.[30−35] Such enclosed ZIF units offer physical protection against external disturbance, further improving their stability, fluorescence behaviors, or sensing performances.[36−38] These superior properties of ZIF-armored materials are intrinsically attributed to well-defined cavities of ZIF that provide the confined freedom and microenvironment for nanoparticles.[39,40] Thus, the introduction of AuNCs into the ZIF templates to make AuNCs@ZIF can efficiently modulate the AIE effect to improve fluorescence behaviors. Combining the advantages of hydrogel with AuNCs@ZIF to fabricate a POC device significantly improves the sensing performance. (i) ZIF encapsulation can restrain intramolecular movement of AuNCs to achieve AIE and protect AuNCs from an external disturbance for the improvement of stability, allowing for hydrogel to directly load AuNCs@ZIF nanocomposites. (ii) The stimuli-responsive properties and semisolid characteristics of AIE-active hydrogel are suitable to shape on a support to facilitate the fabrication of a practical POC device.

Herein, we construct a stable and bright fluorescent AIE-active hydrogel, performing tunable fluorescence behaviors and stimuli-responsive properties (Scheme 1). The AIE-active hydrogel integrates the AIE effect of AuNCs and the porous structure of double-network hydrogels, resulting in a significant boost of the optical response. Harnessing the nanoarchitectures and characteristics, AIE-active hydrogel is cast into gel discs as a fluorescence POC platform to enhance their operational stability and antifouling performance. Combined with high-affinity acetylcholinesterase (AChE), AIE-active hydrogel improves the sensitivity in the assessment and monitoring of chlorpyrifos pesticide. We demonstrate the practicability of POC measurements by imaging gel discs with a smartphone-based portable device to accurately quantitate the degradation of pesticides, providing a promising tool for the development of precision agriculture.

Scheme 1. Schematic Illustrations of AIE-Active Hydrogel Discs for Pesticide Detection

RESULTS AND DISCUSSION

Structural Characterization of AuNCs@ZIF. The preparation of AuNCs@ZIF is schematically illustrated in Figure 1a. Fluorescent AuNCs (as the raw nanomaterial) were prepared using glutathione as the reductant and stabilizer (Figures S1 and S2). Through the coordination action between Zn(II) and the carboxyl group of glutathione or N atom of 2-methylimidazole,[41,42] AuNCs@ZIF composites were successfully obtained and possessed a typical rhombic dodecahedral shape with average diameters of 230 ± 20 nm (Figure 1b). Carefully observed from high-resolution transmission electron microscopy (HRTEM), the AuNCs were predominantly encapsulated in the subsurface region of the composites (Figure 1c). This result was in accordance with the energy-dispersive spectroscopy (EDS) mapping measurement in Figures 1d and S3. Additional evidence of AuNC encapsulation was garnered by confocal laser scanning micrographs of AuNCs@ZIF composites (Figure 1e). The red-emission fluorescence represented the distribution of AuNCs in the resultant composite. Meanwhile, the X-ray diffraction (XRD) measurements substantiated the formation of ZIF-8 in composites, demonstrating that the loading of AuNCs did not influence the crystal growth of ZIF-8 (Figure S4). The Brunauer−Emmett−Teller (BET) analysis revealed a slight decrease in the surface area of AuNCs@ZIF composites (855.3 m^2/g) in comparison with pure ZIF-8 (988.2 m^2/g), further proving that AuNCs were encapsulated in ZIF-8 (Figure 1f). Following the structural characterization of AuNCs@ZIF composites, we set out to measure the brightness of the fluorescent nanostructure. To our delight, the fluorescence intensity of the AuNCs@ZIF composites was enhanced four times in comparison with that of free AuNCs (Figure 1g). The pure ZIF-8 showed no characteristic emission peak at 578 nm, illustrating that the fluorescence characteristics of the composite come from the AuNCs (Figure S5). On the basis of the time-resolved measurement in Figure 1h, the fluorescence lifetime of composites (16.8 μs) was higher than that of free AuNCs (12.8 μs), indicating that the restriction of free movement of the AuNCs suppressed the nonradiative relaxation path and further improved the fluorescence lifetime. X-ray photoelectron spectroscopy (XPS) analysis revealed the presence of Au $4f_{5/2}$ (87.33 eV) and Au $4f_{7/2}$ (83.58 eV) of AuNCs, indicating the enhancement of fluorescence intensity was not induced by the change of the charge state of Au (Figures 1i and S6). Thus, ZIF-8 provided the confined space for AuNCs to reduce the intramolecular vibration and rotation of ligands without changing the charge state of Au,[43,44] efficiently improving the AIE effect by largely suppressing nonradiative relaxation. Furthermore, the chemical stability was investigated by immersing AuNCs@ZIF composites in a high-concentration salt solution and dimethylformamide for 1 h. As expected, the fluorescence intensity of free AuNCs was influenced, while AuNCs@ZIF composites showed negligible fluctuations (Figures S7−S9). These findings suggest that ZIF-8 protects AuNCs from an external disturbance for the improvement of stability. Due to the spatial confinement effects of the ZIF-8, the well-defined AuNCs@ZIF composites showed promising fluorescence performance and chemical stability, making them

https://doi.org/10.1021/acsnano.2c06544
ACS Nano XXXX, XXX, XXX−XXX

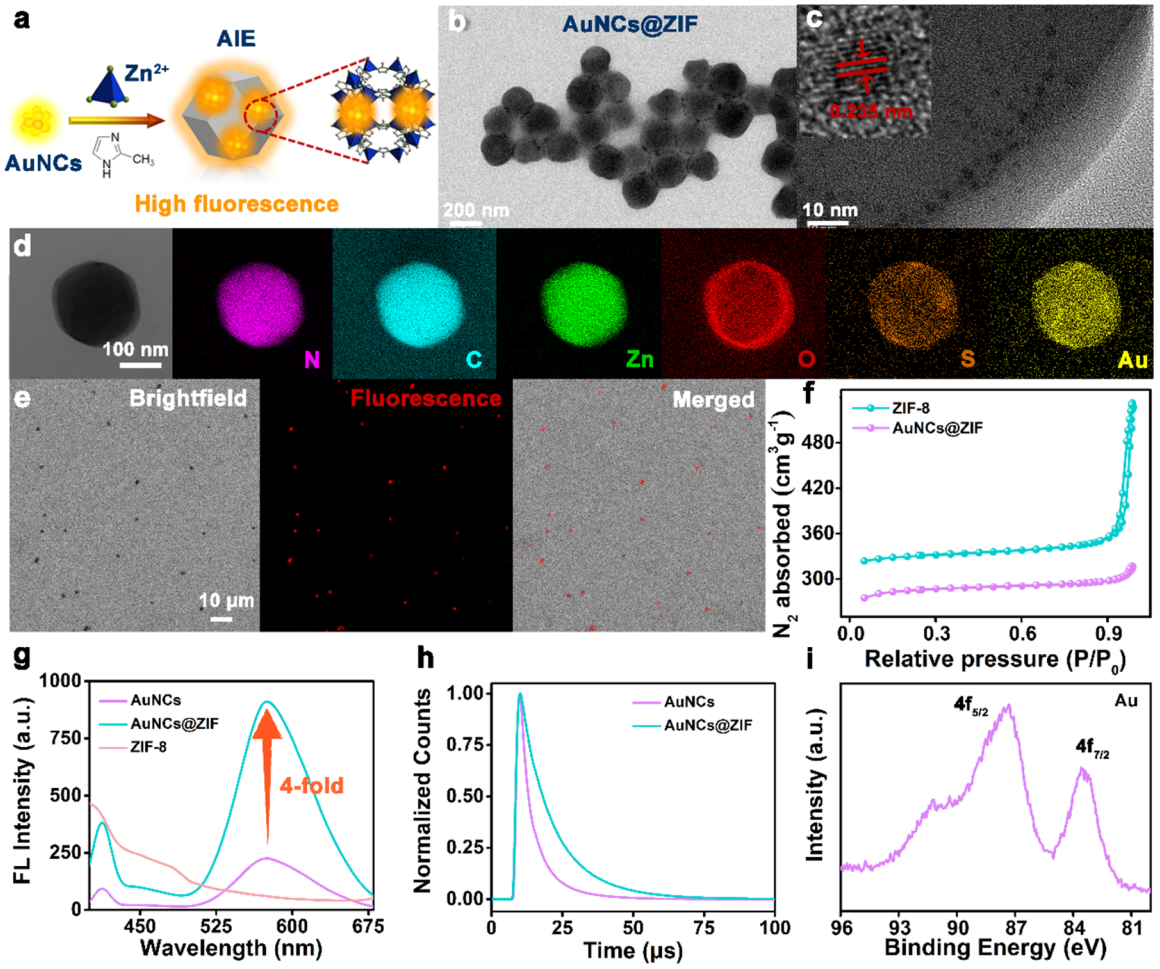

Figure 1. Synthesis and structural characterizations of AuNCs@ZIF. (a) Illustration of the preparation process of AuNCs@ZIF. (b) TEM and (c) HRTEM image of AuNCs@ZIF. (d) Corresponding EDS mapping images of AuNCs@ZIF. (e) Confocal fluorescence microscopy images of AuNCs@ZIF. (f) The BET of AuNCs@ZIF. (g) The fluorescence spectrum of AuNCs and AuNCs@ZIF. (h) The fluorescence lifetime of AuNCs and AuNCs@ZIF. (i) Au 4f XPS spectra of AuNCs@ZIF.

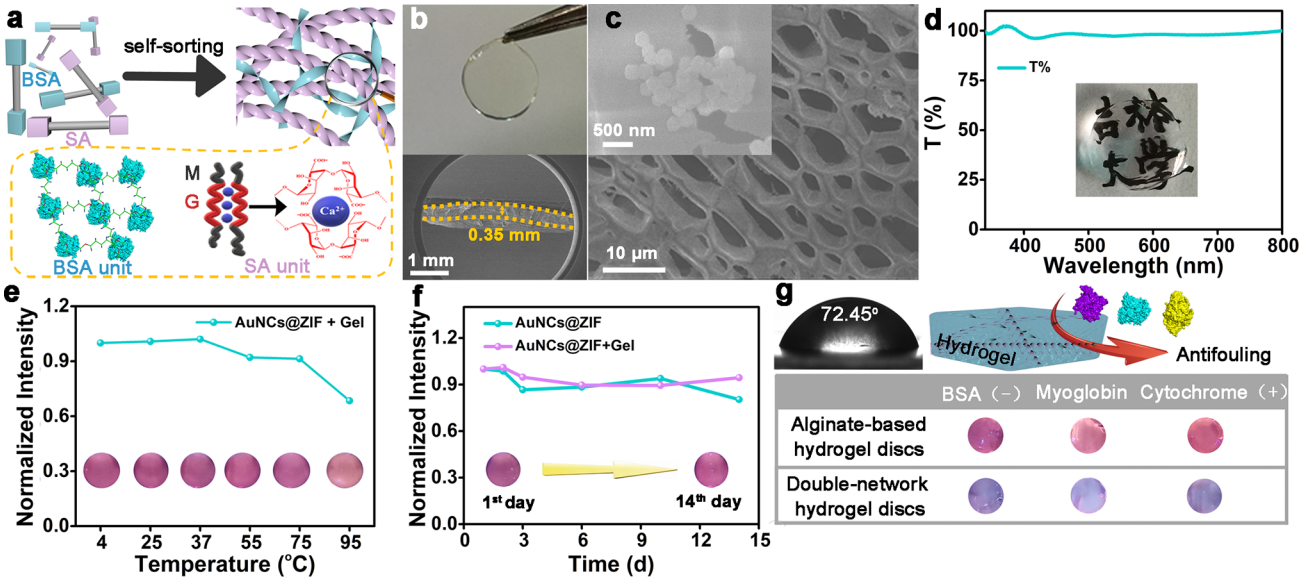

Figure 2. (a) Formation of a double-network hydrogel by the self-sorting assembly of BSA and SA. (b) Image of the hydrogel disc. (c) SEM image of the hydrogel discs. (d) Transmission spectra of the hydrogel disc. (e) Temperature stability of the hydrogel discs. (f) Storage stability of the hydrogel discs. (g) Antifouling performances of the alginate-based hydrogel discs and double-network hydrogel discs.

https://doi.org/10.1021/acsnano.2c06544
ACS Nano XXXX, XXX, XXX−XXX

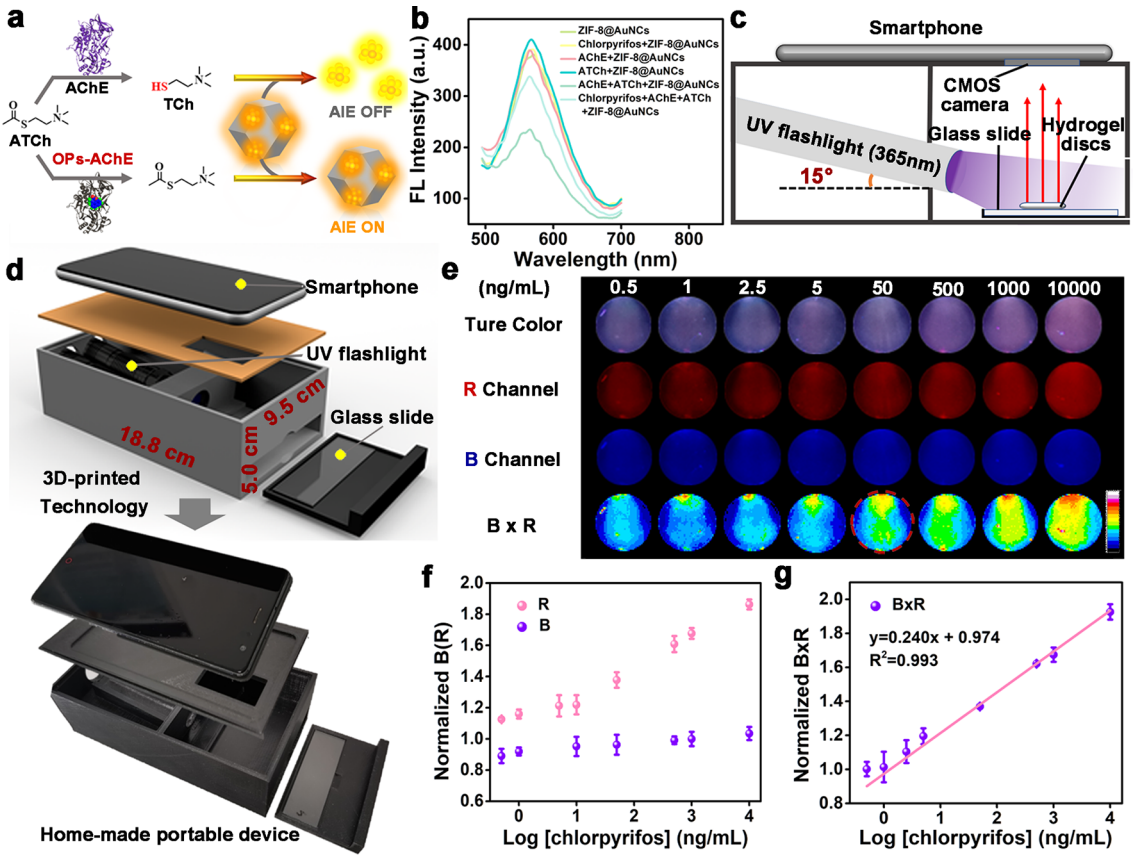

Figure 3. (a) Schematic diagram of the mechanism for the detection of OPs. (b) Fluorescence spectra of the hydrogel with the target. (c) 3D structure design. (d) Illustration of smartphone-based portable fluorescence reading device. (e) True-color images are split into RGB channels, and the B × R response is calculated from pixel arrays of the B and R channels. (f) Normalized intensity of the dependence of B and R values. (g) The relationship of the B × R response with chlorpyrifos concentration.

suitable for mass production, preservation, and practical applications.

Performance Evaluation of AIE-Active Hydrogel. The AIE-active hydrogel was fabricated by embedding the AuNCs@ZIF composites into the hydrogel system through the diffusion hybridization method (Figure 2a). In the coassembly process of constructing stimuli-responsive hydrogel, a double-network structure was obtained from the self-sorting association of glutaraldehyde-cross-linked bovine serum albumin (BSA) and Ca (II)-mediated alginate (SA) junctions. The self-sorting aggregation of the two gelators could enhance intermolecular cooperative interactions, improving the cross-linking strength (Figure S10). The photos of hydrogel discs were in a wet state, and the thickness of the discs was measured to be 0.35 ± 0.04 mm (Figure 2b). The microstructures of the hydrogel were characterized in detail by imaging studies. The scanning electron microscope (SEM) observations indicated that the double-network hydrogels consist of entangled fibers and bond binding to form a dense 3D network (Figure 2c). The transmission spectra of the hydrogel indicated that the light blockage rate almost did not change with the immobilizing AuNCs@ZIF (Figure 2d). The operational stability of hydrogel discs was investigated at different temperatures to evaluate the protective effects of the hydrogel matrix. After the hydrogel discs were exposed to high temperatures (55 and 75 °C), the red emission maintained consistency (Figure 2e), attributed to the protection of AuNCs in the ZIF-8 and hydrogel. The shelf life of AIE-active hydrogel discs was measured during a two-week storage period. Results in Figure 2f indicate that the hydrogel discs with brightness fluorescence possess no degradation over a two-week storage period, suggesting the excellent long-term storage stability of hydrogel discs. Furthermore, the hydrogel discs were immersed in water and stored at −4 °C for 28 days. The red emission fluorescence was mainly distributed in hydrogel discs while no fluorescence was found in the exudate, indicating no leak of the AuNCs@ZIF from the hydrogel within 28 days (Figure S11). Biological fouling is an undesirable effect that blocks the specific signal and reduces assay specificity, causing serious false positives and poor sensitivity.[45] Protein adsorption tests were carried out to assess the antifouling capability of hydrogel discs through incubating with rhodamine B (RhB)-labeled BSA (electric negativity), RhB-labeled myoglobin (electric neutrality), and RhB-labeled cytochrome (electric positivity). Notably, no red emission signal can be observed on the double-network hydrogel discs that hold a relatively clean surface after being incubated with RhB-labeled protein for 30 min, revealing the excellent resistance to the nonspecific protein adsorption by the double-network hydrogels with BSA and SA (Figure 2g). According to the water contact angle data (72.45°), the hydrogel biointerface possessed good hydrophilicity, generating a strongly bound hydration layer to prevent interfacial fouling.[46] Furthermore, BSA as a blocking reagent is widely used to resist nonspecific protein adsorption and passivate biosensor surfaces,[47] largely due to its good inert property and tight surface bonding. Collectively, the excellent

https://doi.org/10.1021/acsnano.2c06544
ACS Nano XXXX, XXX, XXX−XXX

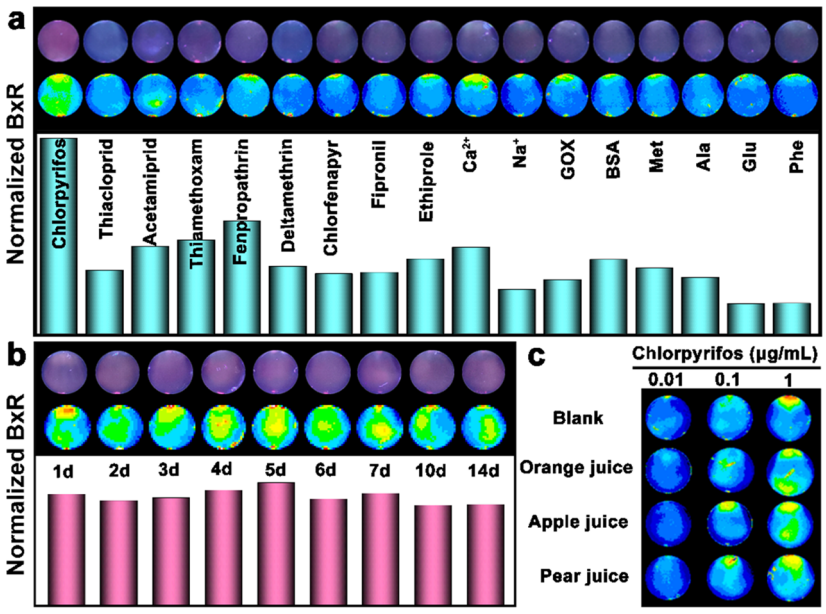

Figure 4. (a) Selectivity performance of hydrogel discs. B × R response of hydrogel discs with interfering substances. (b) Working stability of hydrogel discs toward 1.0 μg/mL chlorpyrifos within 14 days. (c) Fluorescence image of hydrogel discs with spiked fruit juice.

antifouling performance could be attributed to the surface passivation of cross-linked BSA and hydrophilic biointerfaces of the hydrogel.

Hydrogel Disc-Enhanced Sensing Platform. The splendid nature of the AIE-active hydrogel discs is favorable to fabricate an accurate and reliable enzyme-based biosensor (Figure 3a). Specifically, the assembled AuNCs@ZIF collapsed as the enzymatic product thiocholine (TCh), which was obtained by acetylcholinesterase (AChE)-catalyzed hydrolysis of acetylthiocholine (ATCh), was introduced. Compared to the initial AuNCs@ZIF, the typical rhombic dodecahedral shape started to decompose and the AuNCs began to fall off of the framework (Figure S12). When chlorpyrifos was taken as a representative analyte, AChE was irreversibly inactivated and the decomposition of ZIF was blocked, accompanying a distinguishable fluorescence color change (Figures 3b and S13). Thus, chlorpyrifos indirectly regulates the AIE effect of the AuNCs, which can be quantified on the basis of a dynamic scanning optical system that limited its on-site application. In order to simplify the system, we fabricated a portable device with a size of 188 mm × 95 mm × 50 mm (length × width × height) that consists of a smartphone, a 3D-printed accessory, and a light-emitting diode (Figure 3c,d). The relative position of the light source−sample−camera was reasonably fixed in a 3D accessory to account for instability limits during image acquisition. The commercial light-emitting diode (2.5 mW/cm^2) illuminated the hydrogel discs at an incidence angle of 15°, which reduced the background noise of excitation light leakage. The portable device can directly record the fluorescence color (signal) by the built-in complementary metal-oxide semiconductor (CMOS) sensor of the smartphone rather than measuring the fluorescence intensity, which facilitated on-site application. It is worth noting that the microlens of the smartphone not only achieves the image recording of 1:1 but also senses weak light intensity, favoring the acquisition of the high-quality image. The top panel of Figure 3e showed the true-color images of hydrogel discs captured by the portable device. The hydrogel discs had a distinguishable fluorescence color change from blue to red as the chlorpyrifos concentration increased (0.5 to 10 000 ng/mL). To obtain more accurate information from the images, the projected signals (fluorescence color) can be split into three primary color codes (RGB: red, green, blue) by the image-processing algorithm.[48−50] The blue and red signals of the hydrogel discs were enhanced with an increasing chlorpyrifos concentration under optimal conditions (Figures 3f and S14−S16), obtaining a dual-signal fluorescence change. Signals were standardized (B × R) by multiplying the blue intensity values with the red channel to obtain pseudo colors (bottom panel of Figure 3e), which enhanced the accuracy and sensitivity of the corresponding color via amplifying the response signal. This pseudo color shift was advantageous to rapid testing because a chlorpyrifos concentration higher than 50 ng/mL with an apparent green color indicated the residues exceed the maximum residue limits (GB 2763-2021). The fitted curve between the B × R and chlorpyrifos concentration (0.5−10 000 ng/mL) corresponded to a linear equation: y = 0.974 + 0.240 Log[chlorpyrifos] (Figure 3g). Notably, the detection limit (LOD) of the B × R response was calculated to be 0.2 ng/mL, which was 20-fold and 37.5-fold lower than other signal response sensors (Figure S17), confirming the superiority of the B × R response. When the fluorescence color instead of the fluorescence intensity is directly identified, the RGB-based image analysis can improve the accuracy of the test results. In comparison to the different optical sensors for the detection of organophosphorus pesticides (Table S1), the fabricated hydrogel discs displayed promising performance in the sensitivity, detection time, and portability, realizing the quantitative alert for the presence of chlorpyrifos at a particular moment.

The selectivity of hydrogel discs for chlorpyrifos recognition was investigated by introducing several general pesticides, ions, and biomolecules as negative controls. The fluorescence images of hydrogel discs were collected using a homemade portable device (Figure 4a). Even when a 5-fold higher concentration (5.0 μg/mL) than that of chlorpyrifos was introduced, the B × R response of the interferences was still ignorable and the color was consistent with the blank control,

https://doi.org/10.1021/acsnano.2c06544
ACS Nano XXXX, XXX, XXX−XXX

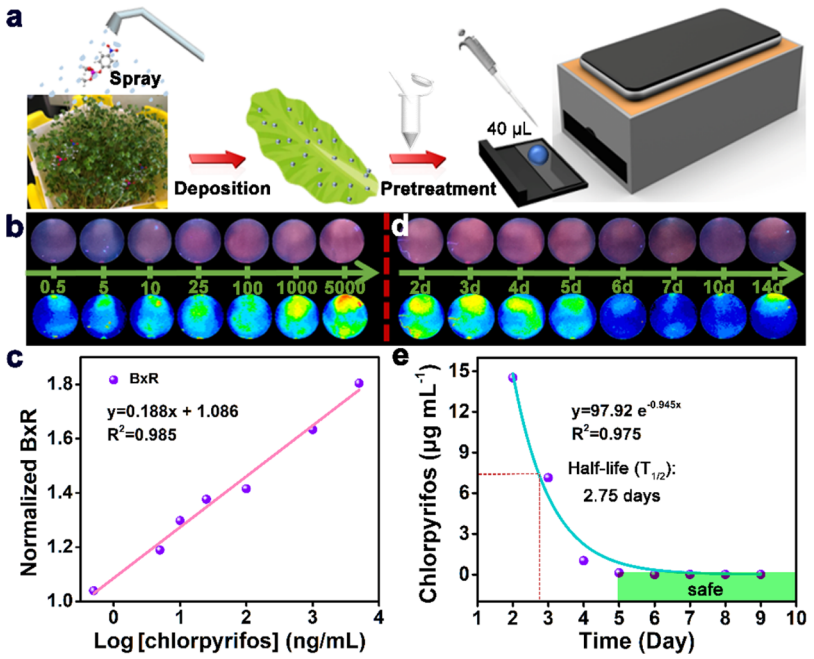

Figure 5. (a) Operation procedure of the hydrogel sensing platform for pesticide degradation. (b) B × R response of the hydrogel discs with chlorpyrifos in the leaves matrix. (c) The working performance of the hydrogel discs in the leaves matrix. (d) B × R response of the hydrogel discs with chlorpyrifos in the leaves. (e) Degradation of chlorpyrifos in the leaves within 10 days.

suggesting the high selectivity of hydrogel discs for chlorpyrifos. Furthermore, coexisting substances and chlorpyrifos were dripped into hydrogel discs to study the anti-interference performance. As compared in Figure S18, the fluorescent color of the hydrogel discs turned from blue to red, indicating that the coexisting substances do not influence the recognition of the sensor. As expected, this result was in accordance with the obtained B × R response of the hydrogel discs. Such a good performance might result from the recognition specificity of AChE and the protection from double-network hydrogels that imposed a restriction on the size of the entering substance. The shelf life of the hydrogel discs was further researched during a two-week storage period at 4 °C and then tested using 25 μL of pesticide (1.0 μg/mL). The as-prepared hydrogel discs exhibited outstanding stability over this two-week storage period (Figure 4b), suggesting that AIE-active hydrogel discs are suitable for storage and transportation. To estimate the practical usability and reliability of hydrogel discs, fruit juices (pear, apple, and orange) containing different concentrations of chlorpyrifos were analyzed three times using hydrogel discs. As depicted in Figure 4c and Table S2, the recovery rates fell in a range from 89.70% to 114.69% with relative standard deviations lower than 5.37%, which possess a good relevance to that of gas chromatography (GC), implying an acceptable accuracy for quantitative chlorpyrifos detection. The precision of the sensor is confirmed by ten parallel experiments, which possess relative standard deviations lower than 4.53% (Figure S19). Such excellent performance for pesticide sensing can be ascribed to these characteristics: (i) ZIF-8 provides the confined space for AuNCs to reduce the intramolecular vibration and rotation of ligands, triggering the AIE effect of the AuNCs and enhancing the fluorescence signal to improve the signal-to-noise ratio. (ii) The AuNCs@ZIF-based hydrogel discs with a double-network structure possess high stability and antifouling performance via surface passivation and hydrophilic biointerfaces of the hydrogel, demonstrating a good protective effect against complex environments. (iii) The proposed platform needs an extremely small volume (as low as 25 μL) to quantitatively analyze chlorpyrifos, which contributed to detecting trace samples with low abundance. Because AChE is one of the most expensive components in this sensing platform, the hydrogel discs required less AChE than other AChE-based systems,[51,52] implying significant cost savings. Furthermore, the current hydrogel discs offer a distinct advantage over conventional POC approaches (only show yes/no) as an accurate quantitative answer using a smartphone-based portable fluorescence reading device.

Monitoring of Pesticides Degradation. Understanding the behavior of pesticide degradation is conducive to fine-tuning the resource inputs, which is of great instructive significance for enhancing pesticide utilization efficiency and reducing pesticide exposures. The sensors are intended to monitor plant health by profiling trait pesticides, which is beneficial to enabling sustainable agricultural production.[53−55] We evaluated the performance of the hydrogel discs by timely monitoring the degradation of pesticides in Chinese cabbages using the portable device (Figure 5a). To correctly investigate pesticide degradation, the working equation was fitted in the Chinese cabbage matrix (Figure 5b,c), which can be used to quantify chlorpyrifos residues. Such good feasibility of a portable device made it suitable to observe the pesticide residues in Chinese cabbages during a 14-day growth stage. As shown in Figure 5d, the chlorpyrifos residues in the leaves of Chinese cabbages were monitored by the on-site recording of the fluorescence color of the hydrogel discs. The results of the portable device showed that large amounts of chlorpyrifos residues (14.5 μg/mL) were found in the leaves after spraying. With the time being prolonged, the B × R response of the leaves increased with pseudo color variation from yellow to blue, indicating that the residues had gradually degraded. The degradation of chlorpyrifos in the leaves followed pseudo-first-

https://doi.org/10.1021/acsnano.2c06544
ACS Nano XXXX, XXX, XXX−XXX

order kinetics, $y = 97.92e^{-0.945x}$ (Figure 5e), which possessed a half-life ($T_{1/2}$) of 2.75 days. Good correlations were obtained between the hydrogel discs and gas chromatography (R^2 = 0.985, Figure S20). Thus, the hydrogel discs possessed sensitive quantitative performance in a convenient and rapid manner. Such hydrogel discs with favorable sensitivity, accuracy, and stability were conducive to understanding the pesticide degradation process and judging the credible picking period for agricultural products, making the portable device a promising candidate for pesticide-related food safety risk assessment during the whole plant growth.

CONCLUSIONS

In summary, we have successfully developed AIE-active hydrogel discs for the acquisition of pesticide residue information in a sensitive manner. During gelation, AuNCs@ZIF composites are embedded into the double-network structure of glutaraldehyde-cross-linked BSA and Ca(II)-mediated alginate self-sorting junctions, possessing distinctive AIE behavior and operational stability. Notably, the cross-linked BSA empowered the double-network hydrogel with an excellent antifouling ability of the recognition interface, which was a practical and important property. On the basis of the high-affinity of AChE, hydrogel discs exhibit a good linear relationship range from 0.5 to 10 000 ng/mL chlorpyrifos pesticide. Using a homemade portable device composed of a 3D-printed accessory and smartphone, the fluorescence images of hydrogel discs were converted into data information, which reflected the accurate quantitation of chlorpyrifos pesticide with a LOD of 0.2 ng/mL. Along with the improved bioanalytical parameters (particularly in terms of detection sensitivity, antifouling performance, and stability), hydrogel discs also shorten the overall assay time, reduce reagent consumption, and simplify the readout instrumentation for on-site testing. More importantly, the portable device was utilized to examine the dynamic degradation of chlorpyrifos in Chinese cabbages. Together, this work provides a plant health sensor for on-site quantification of pesticide residue, satisfying the long-time monitoring during the whole growth period for enhancing pesticide utilization efficiency and reducing pesticide exposures. We envision that, coupling with a homemade device, the AIE-active hydrogel discs will promote the development of precision agriculture.

EXPERIMENTAL SECTION

Preparation of AuNCs@ZIF. AuNCs@ZIF were synthesized by adding zinc acetate (38 mg) and 2-methyl-imidazole (380 mg) into 4.0 mL of ultrapure water with 1.0 mL of a AuNC solution under stirring (400 rpm/min) conditions for 30 min at room temperature. The light-yellow precipitate was collected by centrifugation at 6000 rpm for 5 min and washed three times with ultrawater. Finally, the recovered precipitate was dissolved in 1.0 mL of ultrawater and stored at 4 °C. Pure ZIF-8 was also prepared by a similar procedure in the absence of AuNCs.

Preparation of Hydrogel Discs for Chlorpyrifos Detection. To make the hydrogel discs, we made a master mold for casting the gel discs using a quartz slide. The master mold holds two rows of wells 7 mm in diameter and 0.9 mm in depth to create gel discs. A double cross-linking reaction including 4.5% bovine serum albumin (BSA), 1% sodium alginate, and 0.5% glutaraldehyde in deionized water (pH = 7) was performed. The hydrogels and AuNCs@ZIF mixture were loaded into a well using a pipet followed by immersing into a $CaCl_2$ (0.01 M) solution for 3 min. The hydrogel discs were released from the master mold manually using forceps and stored with ultrawater. These hydrogel discs were then assembled onto a glass slide (76.2 mm × 25.4 mm), at which point they became ready for testing (Figure S21). Various concentrations of the chlorpyrifos standard (25 μL) and 1.0 U/mL AChE (10 μL) were mixed for incubating for 20 min. Then, 50 mmol/L ATCh (10 μL) dissolved in 10 mmol/L HEPES buffer (5.0 μL, pH = 8) was added and incubated for 20 min at 37 °C. 40 μL of the reaction solution was dispensed onto the gel discs. The liquid was allowed to cover, spread, and diffuse throughout the entire gel discs by capillary action. After that, the discs were placed into a portable device. The image was collected and then analyzed using the commercial software ImageJ to analyze the data information on the gel discs.

Preparation of RhB-Labeled Protein. RhB was attached to the protein in sodium bicarbonate buffer (10 mmol L^{-1}, pH = 9.0) with stirring conditions in the dark for 12 h. The concentration of modified protein was 5.0 mg mL^{-1}, and the mixture was labeled with a RhB solution in 10% dimethyl sulfoxide (DMSO, 0.5 mg mL^{-1}). Then, dialysis was used to remove the unreacted RhB.

Real Sample Detection. Fruit juice was processed by a juicer; then, the samples were spiked with 0.01, 0.1, and 1 μg mL^{-1} chlorpyrifos. The spiked samples were mixed with 10 mL of acetonitrile, ultrasonically extracted for 5 min, shaken for 30 min, and centrifuged for 10 min at 4000 rpm. The organic phase was diluted with PBS buffer (10.0 mmol L^{-1}, pH = 8.0) and detected using the current strategy and gas chromatography.

ASSOCIATED CONTENT

Supporting Information

The Supporting Information is available free of charge at https://pubs.acs.org/doi/10.1021/acsnano.2c06544.

Experimental details; TEM images; XRD pattern; XPS and UV−vis absorption spectra, the fluorescence spectrum of AuNCs@ZIF composites; SEM and stability of the hydrogel; the operation, optimization, and anti-interference ability of the hydrogel discs; repeatability and figure of merit of recent works (PDF)

AUTHOR INFORMATION

Corresponding Authors

Xu Yan − *State Key Laboratory of Integrated Optoelectronics, Key Laboratory of Advanced Gas Sensors, Jilin Province, College of Electronic Science and Engineering, Jilin University, Changchun 130012, P. R. China;* orcid.org/0000-0003-2152-675X; Email: yanx@jlu.edu.cn

Geyu Lu − *State Key Laboratory of Integrated Optoelectronics, Key Laboratory of Advanced Gas Sensors, Jilin Province, College of Electronic Science and Engineering and International Center of Future Science, Jilin University, Changchun 130012, P. R. China;* orcid.org/0000-0002-7428-2456; Email: lugy@jlu.edu.cn

Authors

Tuhui Wang − *State Key Laboratory of Integrated Optoelectronics, Key Laboratory of Advanced Gas Sensors, Jilin Province, College of Electronic Science and Engineering, Jilin University, Changchun 130012, P. R. China; Department of Thoracic Surgery, China−Japan Union Hospital, Jilin University, Changchun 130033, P. R. China*

Hongxia Li − *Department of Food Quality and Safety, College of Food Science and Engineering, Jilin University, Changchun 130062, P. R. China;* orcid.org/0000-0003-4240-2027

Lening Zhang − *Department of Thoracic Surgery, China−Japan Union Hospital, Jilin University, Changchun 130033, P. R. China*

https://doi.org/10.1021/acsnano.2c06544
ACS Nano XXXX, XXX, XXX−XXX

Hua Xin − *Department of Thoracic Surgery, China−Japan Union Hospital, Jilin University, Changchun 130033, P. R. China*

Complete contact information is available at: https://pubs.acs.org/10.1021/acsnano.2c06544

Author Contributions

[▽]X.Y. and T.W. contributed equally to this work.

Notes

The authors declare no competing financial interest.

ACKNOWLEDGMENTS

The authors would like to acknowledge the financial support by the National Natural Science Foundation of China (62171194, 31901777, and 61831011), the Natural Science Foundation of Jilin Province (20200201218JC and 20220402054GH), and the Interdisciplinary Innovation Cultivation Project of Jilin University (JLUXKJC2020315). We would like to acknowledge Dr. Dong Yao (Jilin University) for helpful comments.

REFERENCES

(1) Culver, H. R.; Clegg, J. R.; Peppas, N. A. Analyte-Responsive Hydrogels: Intelligent Materials for Biosensing and Drug Delivery. *Acc. Chem. Res.* **2017**, *50*, 170−178.

(2) Fenton, O. S.; Olafson, K. N.; Pillai, P. S.; Mitchell, M. J.; Langer, R. Advances in Biomaterials for Drug Delivery. *Adv. Mater.* **2018**, *30*, 1705328.

(3) Zhu, C.; Fu, Y. J.; Liu, C. A.; Liu, Y.; Hu, L. L.; Liu, J.; Bello, I.; Li, H.; Liu, N. Y.; Guo, S. J.; Huang, H.; Lifshitz, Y.; Lee, S. T.; Kang, Z. H. Carbon Dots as Fillers Inducing Healing/Self-Healing and Anticorrosion Properties in Polymers. *Adv. Mater.* **2017**, *29*, 1701399.

(4) Chen, W. H.; Liao, W. C.; Sohn, Y. S.; Fadeev, M.; Cecconello, A.; Nechushtai, R.; Willner, I. Stimuli-Responsive Nucleic Acid-Based Polyacrylamide Hydrogel-Coated Metal-Organic Framework Nanoparticles for Controlled Drug Release. *Adv. Funct. Mater.* **2018**, *28*, 1705137.

(5) Liang, Y.; He, J.; Guo, B. Functional Hydrogels as Wound Dressing to Enhance Wound Healing. *ACS Nano* **2021**, *15*, 12687−12722.

(6) Yang, C. H.; Suo, Z. G. Hydrogel Ionotronics. *Nat. Rev. Mater.* **2018**, *3*, 125−142.

(7) Niazi, M.; Alizadeh, E.; Zarebkohan, A.; Seidi, K.; Ayoubi-Joshaghani, M. H.; Azizi, M.; Dadashi, H.; Mahmudi, H.; Javaheri, T.; Jaymand, M.; Hamblin, M. R.; Jahanban-Esfahlan, R.; Amoozgar, Z. Advanced Bioresponsive Multitasking Hydrogels in the New Era of Biomedicine. *Adv. Funct. Mater.* **2021**, *31*, 2104123.

(8) Zhong, R. B.; Tang, Q.; Wang, S. P.; Zhang, H. B.; Zhang, F.; Xiao, M. S.; Man, T. T.; Qu, X. M.; Li, L.; Zhang, W. J.; Pei, H. Self-Assembly of Enzyme-Like Nanofibrous G-Molecular Hydrogel for Printed Flexible Electrochemical Sensors. *Adv. Mater.* **2018**, *30*, 1706887.

(9) Rong, Q. F.; Lei, W. W.; Chen, L.; Yin, Y. A.; Zhou, J. J.; Liu, M. J. Anti-Freezing, Conductive Self-Healing Organohydrogels with Stable Strain-Sensitivity at Subzero Temperatures. *Angew. Chem., Int. Ed.* **2017**, *56*, 14159−14163.

(10) Qin, M.; Sun, M.; Bai, R. B.; Mao, Y. Q.; Qian, X. S.; Sikka, D.; Zhao, Y.; Qi, H. J.; Suo, Z. G.; He, X. M. Bioinspired Hydrogel Interferometer for Adaptive Coloration and Chemical Sensing. *Adv. Mater.* **2018**, *30*, 1800468.

(11) Wang, G. F.; Li, Y. S.; Cai, Z. Z.; Dou, X. C. A Colorimetric Artificial Olfactory System for Airborne Improvised Explosive Identification. *Adv. Mater.* **2020**, *32*, 1907043.

(12) Willner, I. Stimuli-Controlled Hydrogels and Their Applications. *Acc. Chem. Res.* **2017**, *50*, 657−658.

(13) Li, P. P.; Jin, Z. Y.; Peng, L. L.; Zhao, F.; Xiao, D.; Jin, Y.; Yu, G. H. Stretchable All-Gel-State Fiber-Shaped Supercapacitors Enabled by Macromolecularly Interconnected 3D Graphene/Nanostructured Conductive Polymer Hydrogels. *Adv. Mater.* **2018**, *30*, 1800124.

(14) Okesola, B. O.; Mendoza-Martinez, A. K.; Cidonio, G.; Derkus, B.; Boccorh, D. K.; Osuna de la Pena, D.; Elsharkawy, S.; Wu, Y.; Dawson, J. I.; Wark, A. W.; Knani, D.; Adams, D. J.; Oreffo, R. O. C.; Mata, A. De Novo Design of Functional Coassembling Organic-Inorganic Hydrogels for Hierarchical Mineralization and Neovascularization. *ACS Nano* **2021**, *15*, 11202−11217.

(15) Yuan, J.; Wen, D.; Gaponik, N.; Eychmuller, A. Enzyme-Encapsulating Quantum Dot Hydrogels and Xerogels as Biosensors: Multifunctional Platforms for Both Biocatalysis and Fluorescent Probing. *Angew. Chem.* **2013**, *52*, 976−979.

(16) Won, H. J.; Ryplida, B.; Kim, S. G.; Lee, G.; Ryu, J. H.; Park, S. Y. Diselenide-Bridged Carbon-Dot-Mediated Self-Healing, Conductive, and Adhesive Wireless Hydrogel Sensors for Label-Free Breast Cancer Detection. *ACS Nano* **2020**, *14*, 8409−8420.

(17) Guo, J. J.; Liu, X. Y.; Jiang, N.; Yetisen, A. K.; Yuk, H.; Yang, C. X.; Khademhosseini, A.; Zhao, X. H.; Yun, S. H. Highly Stretchable, Strain Sensing Hydrogel Optical Fibers. *Adv. Mater.* **2016**, *28*, 10244−10249.

(18) Zhang, H.; Guo, J.; Wang, Y.; Sun, L.; Zhao, Y. Stretchable and Conductive Composite Structural Color Hydrogel Films as Bionic Electronic Skins. *Adv. Sci.* **2021**, *8*, No. 2102156.

(19) Zheng, K. K.; Tong, Y.; Zhang, S. H.; He, R. Y.; Xiao, L.; Iqbal, Z.; Zhang, Y. H.; Gao, J.; Zhang, L.; Jiang, L. B.; Li, Y. L. Flexible Bicolorimetric Polyacrylamide/Chitosan Hydrogels for Smart Real-Time Monitoring and Promotion of Wound Healing. *Adv. Funct. Mater.* **2021**, *31*, 2102599.

(20) Hu, Y. B.; Barbier, L.; Li, Z.; Ji, X. F.; Le Blay, H.; Hourdet, D.; Sanson, N.; Lam, J. W. Y.; Marcellan, A.; Tang, B. Z. Hydrophilicity-Hydrophobicity Transformation, Thermoresponsive Morphomechanics, and Crack Multifurcation Revealed by AIEgens in Mechanically Strong Hydrogels. *Adv. Mater.* **2021**, *33*, 2101500.

(21) Jiang, H.; Qin, Z. J.; Zheng, Y. K.; Liu, L.; Wang, X. M. Aggregation-Induced Electrochemiluminescence by Metal-Binding Protein Responsive Hydrogel Scaffolds. *Small* **2019**, *15*, 1901170.

(22) Qian, J.; Tang, B. Z. AIE Luminogens for Bioimaging and Theranostics: From Organelles to Animals. *Chem.* **2017**, *3*, 56−91.

(23) Wu, Z. N.; Yao, Q. F.; Chai, O. J. H.; Ding, N.; Xu, W.; Zang, S. Q.; Xie, J. P. Unraveling the Impact of Gold(I)-Thiolate Motifs on the Aggregation-Induced Emission of Gold Nanoclusters. *Angew. Chem., Int. Ed.* **2020**, *59*, 9934−9939.

(24) Wang, X. R.; Hu, J. M.; Zhang, G. Y.; Liu, S. Y. Highly Selective Fluorogenic Multianalyte Biosensors Constructed via Enzyme-Catalyzed Coupling and Aggregation-Induced Emission. *J. Am. Chem. Soc.* **2014**, *136*, 9890−9893.

(25) Feng, G. X.; Liu, B. Aggregation-Induced Emission (AIE) Dots: Emerging Theranostic Nanolights. *Acc. Chem. Res.* **2018**, *51*, 1404−1414.

(26) Xie, Z. C.; Sun, P. P.; Wang, Z.; Li, H. G.; Yu, L. Y.; Sun, D.; Chen, M. J.; Bi, Y. T.; Xin, X.; Hao, J. C. Metal-Organic Gels from Silver Nanoclusters with Aggregation-Induced Emission and Fluorescence-to-Phosphorescence Switching. *Angew. Chem., Int. Ed.* **2020**, *59*, 9922−9927.

(27) Goswami, N.; Lin, F. X.; Liu, Y. B.; Leong, D. T.; Xie, J. P. Highly Luminescent Thiolated Gold Nanoclusters Impregnated in Nanogel. *Chem. Mater.* **2016**, *28*, 4009−4016.

(28) Wang, H.; Zhao, E. G.; Lam, J. W. Y.; Tang, B. Z. AIE Luminogens: Emission Brightened by Aggregation. *Mater. Today* **2015**, *18*, 365−377.

(29) Li, Z.; Ji, X. F.; Xie, H. L.; Tang, B. Z. Aggregation-Induced Emission-Active Gels: Fabrications, Functions, and Applications. *Adv. Mater.* **2021**, *33*, 2100021.

(30) Dhakshinamoorthy, A.; Garcia, H. Catalysis by Metal Nanoparticles Embedded on Metal-Organic Frameworks. *Chem. Soc. Rev.* **2012**, *41*, 5262−5284.

(31) Luo, Y. C.; Fan, S. Y.; Yu, W. Q.; Wu, Z. L.; Cullen, D. A.; Liang, C. L.; Shi, J. Y.; Su, C. Y. Fabrication of Au-25(SG)(18)-ZIF-8 Nanocomposites: A Facile Strategy to Position Au-25(SG)(18) Nanoclusters Inside and Outside ZIF-8. *Adv. Mater.* **2018**, *30* (6), 1704576.
(32) Li, M.; Qiao, S.; Zheng, Y.; Andaloussi, Y. H.; Li, X.; Zhang, Z.; Li, A.; Cheng, P.; Ma, S.; Chen, Y. Fabricating Covalent Organic Framework Capsules with Commodious Microenvironment for Enzymes. *J. Am. Chem. Soc.* **2020**, *142*, 6675−6681.
(33) Chen, W. H.; Vazquez-Gonzalez, M.; Zoabi, A.; Abu-Reziq, R.; Willner, I. Biocatalytic Cascades Driven by Enzymes Encapsulated in Metal-Organic Framework Nanoparticles. *Nat. Catal.* **2018**, *1*, 689−695.
(34) Hu, C.; Bai, Y. X.; Hou, M.; Wang, Y. S.; Wang, L. C.; Cao, X.; Chan, C.; Sun, H.; Li, W. B.; Ge, J.; Ren, K. N. Defect-Induced Activity Enhancement of Enzyme-Encapsulated Metal-Organic Frameworks Revealed in Microfluidic Gradient Mixing Synthesis. *Sci. Adv.* **2020**, *6*, eaax5785.
(35) Chen, G. S.; Huang, S. M.; Kou, X. X.; Zhu, F.; Ouyang, G. F. Embedding Functional Biomacromolecules Within Peptide-Directed Metal-Organic Framework (MOF) Nanoarchitectures Enables Activity Enhancement. *Angew. Chem., Int. Ed.* **2020**, *59*, 13947−13954.
(36) Hu, X.; Liu, X. D.; Zhang, X. D.; Chai, H. X.; Huang, Y. M. One-pot Synthesis of the CuNCs/ZIF-8 Nanocomposites for Sensitively Detecting H_2O_2 and Screening of Oxidase Activity. *Biosens. Bioelectron.* **2018**, *105*, 65−70.
(37) Liu, J.; Guo, Z. Y.; Liang, K. Biocatalytic Metal-Organic Framework-Based Artificial Cells. *Adv. Funct. Mater.* **2019**, *29*, 1905321.
(38) Wang, H. R.; Han, L.; Zheng, D.; Yang, M. F.; Andaloussi, Y. H.; Cheng, P.; Zhang, Z. J.; Ma, S. Q.; Zaworotko, M. J.; Feng, Y. F.; Chen, Y. Protein-Structure-Directed Metal-Organic Zeolite-like Networks as Biomacromolecule Carriers. *Angew. Chem., Int. Ed.* **2020**, *59*, 6263−6267.
(39) Wu, S. Y.; Min, H.; Shi, W.; Cheng, P. Multicenter Metal-Organic Framework-Based Ratiometric Fluorescent Sensors. *Adv. Mater.* **2020**, *32*, 1805871.
(40) Li, M. M.; Qiao, S.; Zheng, Y. L.; Andaloussi, Y. H.; Li, X.; Zhang, Z. J.; Li, A.; Cheng, P.; Ma, S. Q.; Chen, Y. Fabricating Covalent Organic Framework Capsules with Commodious Microenvironment for Enzymes. *J. Am. Chem. Soc.* **2020**, *142*, 6675−6681.
(41) Ogata, A. F.; Rakowski, A. M.; Carpenter, B. P.; Fishman, D. A.; Merham, J. G.; Hurst, P. J.; Patterson, J. P. Direct Observation of Amorphous Precursor Phases in the Nucleation of Protein-Metal-Organic Frameworks. *J. Am. Chem. Soc.* **2020**, *142*, 1433−1442.
(42) Liang, K.; Ricco, R.; Doherty, C. M.; Styles, M. J.; Bell, S.; Kirby, N.; Mudie, S.; Haylock, D.; Hill, A. J.; Doonan, C. J.; Falcaro, P. Biomimetic Mineralization of Metal-Organic Frameworks as Protective Coatings for Biomacromolecules. *Nat. Commun.* **2015**, *6*, 7240.
(43) Peng, H. P.; Huang, Z. N.; Deng, H. H.; Wu, W. H.; Huang, K. Y.; Li, Z. L.; Chen, W.; Liu, J. W. Dual Enhancement of Gold Nanocluster Electrochemiluminescence: Electrocatalytic Excitation and Aggregation-Induced Emission. *Angew. Chem., Int. Ed.* **2020**, *59*, 9982−9985.
(44) Yang, L. Q.; Zhang, B.; Fu, L.; Fu, K. N.; Zou, G. Z. Efficient and Monochromatic Electrochemiluminescence of Aqueous-Soluble Au Nanoclusters via Host-Guest Recognition. *Angew. Chem., Int. Ed.* **2019**, *58*, 6901−6905.
(45) Wang, L.; He, E.; Gao, R.; Wu, X. T.; Zhou, A. W.; Lu, J.; Zhao, T.; Li, J. X.; Yun, Y. J.; Li, L. H.; Ye, T. T.; Jiao, Y. D.; Wang, J. C.; Chen, H.; Li, D.; Ning, X. H.; Wu, D.; Peng, H. S.; Zhang, Y. Designing Porous Antifouling Interfaces for High-Power Implantable Biofuel Cell. *Adv. Funct. Mater.* **2021**, *31*, 2107160.
(46) Song, Z.; Ma, Y. H.; Chen, M.; Ambrosi, A.; Ding, C. F.; Luo, X. L. Electrochemical Biosensor with Enhanced Antifouling Capability for COVID-19 Nucleic Acid Detection in Complex Biological Media. *Anal. Chem.* **2021**, *93*, 5963−5971.
(47) Jiang, C.; Wang, G. X.; Hein, R.; Liu, N. Z.; Luo, X. L.; Davis, J. J. Antifouling Strategies for Selective *In Vitro* and *In Vivo* Sensing. *Chem. Rev.* **2020**, *120*, 3852−3889.
(48) Wang, J.; Jiang, C. X.; Jin, J. N.; Huang, L.; Yu, W. B.; Su, B.; Hu, J. Ratiometric Fluorescent Lateral Flow Immunoassay for Point-of-Care Testing of Acute Myocardial Infarction. *Angew. Chem., Int. Ed.* **2021**, *60*, 13042−13049.
(49) Chen, H. B.; Yu, J. B.; Men, X. X.; Zhang, J. C.; Ding, Z. Y.; Jiang, Y. F.; Wu, C. F.; Chiu, D. T. Reversible Ratiometric NADH Sensing Using Semiconducting Polymer Dots. *Angew. Chem., Int. Ed.* **2021**, *60*, 12007−12012.
(50) Sun, K.; Yang, Y. K.; Zhou, H.; Yin, S. Y.; Qin, W. P.; Yu, J. B.; Chiu, D. T.; Yuan, Z.; Zhang, X. J.; Wu, C. F. Ultrabright Polymer-Dot Transducer Enabled Wireless Glucose Monitoring via a Smartphone. *ACS Nano* **2018**, *12*, 5176−5184.
(51) Hu, T.; Xu, J.; Ye, Y.; Han, Y.; Li, X.; Wang, Z.; Sun, D.; Zhou, Y.; Ni, Z. Visual Detection of Mixed Organophosphorous Pesticide using QD-AChE Aerogel Based Microfluidic Arrays Sensor. *Biosens. Bioelectron.* **2019**, *136*, 112−117.
(52) Chen, J.; Chen, X.; Wang, P.; Liu, S.; Chi, Z. Aggregation-Induced Emission Luminogen@manganese Dioxide Core-shell Nanomaterial-Based Paper Analytical Device for Equipment-free and Visual Detection of Organophosphorus Pesticide. *J. Hazard. Mater.* **2021**, *413*, 125306.
(53) Zhang, Q.; Ying, Y. B.; Ping, J. F. Recent Advances in Plant Nanoscience. *Adv. Sci.* **2022**, *9*, 2103414.
(54) Zhao, F. N.; He, J. W.; Li, X. J.; Bai, Y. P.; Ying, Y. B.; Ping, J. F. Smart Plant-Wearable Biosensor for *In-situ* Pesticide Analysis. *Biosens. Bioelectron.* **2020**, *170*, 112636.
(55) Lee, G.; Wei, Q. S.; Zhu, Y. Emerging Wearable Sensors for Plant Health Monitoring. *Adv. Funct. Mater.* **2021**, *31*, 2106475.

https://doi.org/10.1021/acsnano.2c06544
ACS Nano XXXX, XXX, XXX−XXX